Available online at www.sciencedirect.com
SCIENCE DIRECT®
International Journal of Heat and Mass Transfer 47 (2004) 1445–1465
International Journal of HEAT and MASS TRANSFER
www.elsevier.com/locate/ijhmt

Mixed convection heat transfer along a continuously moving heated vertical plate with suction or injection

Sami A. Al-Sanea *

Department of Mechanical Engineering, College of Engineering, King Saud University, P.O. Box 800, Riyadh 11421, Saudi Arabia

Received 21 March 2002

Abstract

The steady laminar flow and heat transfer characteristics of a continuously moving vertical sheet of extruded material are studied close to and far downstream from the extrusion slot. Uniform or non-uniform suction/injection is allowed at the surface. The velocity and temperature variations, obtained by a finite-volume method, are used to map out the entire forced, mixed and natural convection regimes. The effects of the Prandtl number (Pr), the buoyancy force parameter (B) and the suction/injection parameter (D) on the friction and heat transfer coefficients are investigated. Comparisons of results with local-similarity method and finite-difference solutions of the boundary layer equations and with exact analytic solutions for asymptotic suction flows show an excellent agreement. The region close to the extrusion slot is characterized as a diffusion dominated region in which $Nu_xRe_x^{-1/2}$ drops sharply with increasing Richardson number (Ri_x). This is followed by a forced-convection dominated region in which $Nu_xRe_x^{-1/2}$ levels off with increasing Ri_x until the buoyancy effect sets in. A mixed convection region where increasing buoyancy effect enhances the heat transfer rate follows. Finally, this region is followed downstream by a natural-convection dominated region in which $Nu_xRe_x^{-1/2}$ approaches asymptotically the pure natural convection results. For the case of uniform suction and far downstream from the slot, the boundary layer thickness becomes constant and the heat transfer rate approaches a constant asymptotic suction value independent of the heat convection mode. Critical values of Ri_x to distinguish the various convection regimes are determined for different Pr, B and D.

Keywords: Continuously moving surface; Mixed convection; Laminar convection regimes; Suction or injection; Backward boundary layer

1. Introduction

The problem considered in this paper is that of the effects of suction and injection on the laminar mixed-convection heat transfer along a continuously moving plate. The plate emerges vertically upward from an extrusion slot and is held at a constant temperature greater than the temperature of the ambient fluid. Both cases of uniform and non-uniform suction/injection are considered. The flow field is induced by the viscous action of the moving plate, suction/injection at the surface, and thermal buoyancy; the region close to the slot is also influenced by the extrusion die wall. The resulting convection regimes are determined by the relative effect of the buoyancy forces on the heat transfer rate compared to the effect of the viscous and inertia forces.

Thermal transport from a continuously moving heated plate through an otherwise quiescent fluid has many applications in manufacturing processes such as hot rolling, metal and plastic extrusion, continuous casting, and glass fiber and paper production. Knowledge of the flow and thermal fields adjacent to the moving plate is necessary for determining the quality of the final products of these processes, Karwe and Jaluria [1,2]. This physical situation is different from that of the classical boundary-layer flow over a stationary flat plate

* Fax: +966-1-467-6652.
E-mail address: sanea@ksu.edu.sa (S.A. Al-Sanea).

0017-9310/$ - see front matter © 2003 Elsevier Ltd. All rights reserved.
doi:10.1016/j.ijheatmasstransfer.2003.09.016

Nomenclature

B	buoyancy force parameter $= Gr_x/Re_x^3 = g\beta(T_w - T_\infty)v/u_w^3$
c_p	specific heat at constant pressure
$C_{f,x}$	local skin-friction coefficient $= \tau_{w,x}/0.5\rho u_w^2$
D	suction or injection parameter $= v_w/u_w$
D_F	suction or injection parameter $= (v_w x/v)Re_x^{-1/2}$
D_N	suction or injection parameter $= (v_w x/3v)(Gr_x/4)^{-1/4}$
g	gravitational acceleration
Gr_x	local Grashof number $= g\beta(T_w - T_\infty)x^3/v^2$
h_x	local heat-transfer coefficient
k	thermal conductivity of fluid
L	domain length
Nu_x	local Nusselt number $= h_x x/k$
p	pressure
P	dimensionless pressure $= (p - p_\infty)/\rho u_w^2$
Pr	Prandtl number $= v/\alpha$
q_x	local heat flux
Re_x	local Reynolds number $= u_w x/v$
Ri_x	local Richardson number $= Gr_x/Re_x^2 = g\beta(T_w - T_\infty)x/u_w^2$
St_x	local Stanton number $= Nu_x/(Re_x Pr) = h_x/(\rho u_w c_p)$
T	temperature
u	velocity component in x-direction
u_w	plate velocity
U	dimensionless velocity component $= u/u_w$
v	velocity component in y-direction
v_w	suction or injection velocity
V	dimensionless velocity component $= v/u_w$
x	coordinate along direction of surface motion
X	dimensionless coordinate $= x/L$
y	coordinate along direction normal to surface motion
Y	dimensionless coordinate $= y/L$

Greek symbols

α	thermal diffusivity
β	volumetric thermal expansion coefficient
θ	dimensionless temperature $= (T - T_\infty)/(T_w - T_\infty)$
v	kinematic viscosity
ρ	density
$\tau_{w,x}$	local shear stress

Subscripts

c	critical conditions
e	pertains to entrained velocity
F	forced convection
N	natural convection
w	condition at plate surface
∞	condition at ambient medium

(Blasius flow) because of fluid entrainment toward the moving surface. Sakiadis [3,4] was the first to recognize this backward boundary-layer situation and used a similarity transformation to obtain a numerical solution for the flow field of a continuously moving surface.

Since the pioneering work of Sakiadis, many authors have analyzed the hydrodynamic and thermal characteristics of such a class of boundary layer problems for various conditions. Tsou et al. [5] reported, analytically and experimentally, the flow and thermal fields developed by a continuously moving surface and showed that this flow is physically realizable under laboratory conditions. Stretched surfaces with different velocity and temperature conditions at the surface were studied in [6–9].

Suction or injection of fluid through the surface, as in mass transfer cooling, can significantly change the flow field and affect the heat transfer rate from the plate. Suction or injection through a stretched surface was introduced by Erickson et al. [10] and Fox et al. [11] for a uniform surface velocity and temperature, and by Gupta and Gupta [12] and Chen and Char [13] for a linearly varying surface velocity. Power-law velocity and temperature distributions at the surface were studied by Ali [14]. It is noted that the suction or injection velocity must vary along the surface in a power law form if similarity solutions are to be obtained. In general, suction increases the skin-friction and heat-transfer coefficients, whereas injection acts in the opposite manner.

The buoyancy forces resulting from the temperature differences in the fluid can be important if the velocity of the moving surface is relatively low and the temperature difference between the surface and the fluid is large. This can affect significantly the velocity and temperature distributions and, hence, the heat transfer rate from the surface. Neglecting the effect of buoyancy in such situations can, therefore, produce unrealistic results. Buoyancy effects in boundary layers on continuously moving surfaces through an otherwise quiescent fluid have been studied in [15,16] for horizontal surfaces, in [17–19] for vertical surfaces, and in [20–22] for vertical and inclined surfaces. In the presence of buoyancy forces, similarity solutions do not exist except for a restricted power-law surface velocity and temperature distributions. Mixed convection correlations for continuously moving sheets were reviewed by Chen and Armaly [23]. They reported extensive correlations for horizontal, inclined and ver-

tical moving sheets and for both the uniform wall temperature and uniform heat flux boundary conditions. The heat transfer rate was found to increase for the buoyancy-assisting situation and to decrease for the buoyancy-opposing situation.

In almost all the papers cited earlier, the studies concentrated on the boundary layer far away from the extrusion slot where the boundary layer approximations are valid and, hence, similarity and/or local-similarity method solutions may be used. However, the flow and heat transfer characteristics are also important close to the slot where both the friction and heat transfer coefficients attain their largest values. A finite-difference formulation using the full (elliptic) governing equations including buoyancy effects was employed by Karwe and Jaluria [1,2], and Kang and Jaluria [24]. The effect of buoyancy was found to be more prominent when the plate moves vertically upward than when it moves horizontally. It was also found that the elliptic effects are important near the extrusion slot and decay downstream. In these papers, suction or injection through the plate was not considered.

In a recent study, Al-Sanea and Ali [25] investigated the effects of the extrusion die wall and of suction and injection at the moving surface on the friction and heat-transfer coefficient distributions with emphasis on the region close to the extrusion slot using the full elliptic equations. Critical Reynolds numbers to distinguish between the non-similar and self-similar regions were also determined. However, the buoyancy effects were not accounted for and, hence, only the pure forced convection regime was analyzed. Accounting for the buoyancy effects but by treating the surface to be impermeable, Al-Sanea [26] analyzed the entire mixed convection regime for a continuously moving heated vertical plate. Regimes of forced, mixed and natural convection have been mapped as a function of Reynolds and Grashof numbers.

In summary, studies on mixed convection heat transfer along a moving plate with suction or injection are scarce and are limited in the physical sense of employing power law variations of transpiration velocity for which local similarity solutions are possible as were used in [18,19]. Besides, the boundary layer assumptions employed are not valid in the elliptic region that exists close to the extrusion slot.

The present study, therefore, extends the work in [26] and examines the combined effects of buoyancy and surface mass transfer on the flow and thermal characteristics along a continuously moving heated vertical plate. Emphasis is given to the region close to the extrusion slot as well as the entire mixed convection region. Another objective is to determine the critical values of Richardson number ($Ri_{x,c}$) in order to delineate the forced, mixed and natural convection regimes for different values of the Prandtl number (Pr), the buoyancy force parameter (B) and the suction/injection parameter (D).

2. Mathematical formulation and calculation procedure

2.1. Basic assumptions and governing equations

Fig. 1 shows a continuously moving heated vertical plate emerging from a slot at a velocity u_w and a

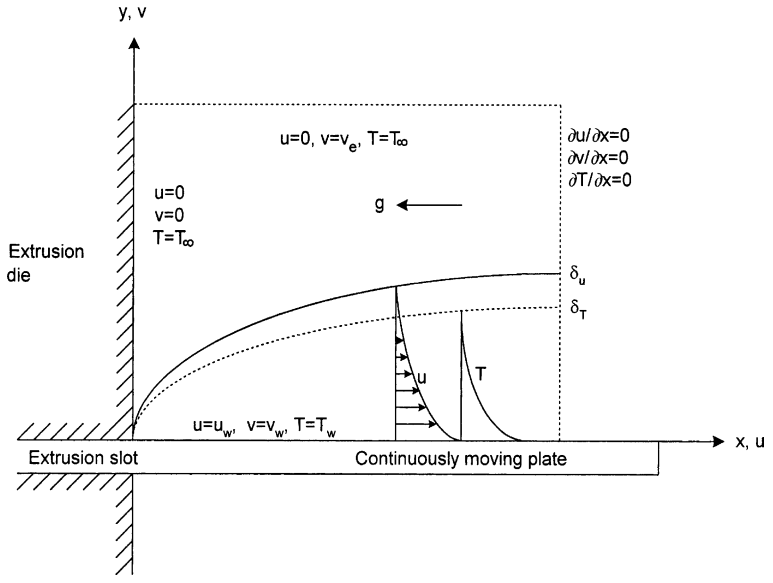

Fig. 1. A schematic showing the physical situation and boundary conditions of a continuously moving plate.

temperature T_w in an otherwise quiescent fluid at temperature T_∞. The gravitational body force is oriented in the negative x direction. Suction or injection is allowed through the plate. The induced motion of the fluid is assumed to be laminar, steady, and two-dimensional with thermally active incompressible viscous fluid with constant properties. Further simplification is made through the use of the Boussinesq approximation. Subject to these assumptions, the full elliptic governing equations can be written as:

$$\frac{\partial U}{\partial X}+\frac{\partial V}{\partial Y}=0 \tag{1}$$

$$\frac{\partial}{\partial X}(U^2)+\frac{\partial}{\partial Y}(UV)-\frac{1}{Re_L}\left(\frac{\partial^2 U}{\partial X^2}+\frac{\partial^2 U}{\partial Y^2}\right) = -\frac{\partial P}{\partial X}+\frac{Gr_L}{Re_L^2}\theta \tag{2}$$

$$\frac{\partial}{\partial X}(UV)+\frac{\partial}{\partial Y}(V^2)-\frac{1}{Re_L}\left(\frac{\partial^2 V}{\partial X^2}+\frac{\partial^2 V}{\partial Y^2}\right)=-\frac{\partial P}{\partial Y} \tag{3}$$

$$\frac{\partial}{\partial X}(U\Theta)+\frac{\partial}{\partial Y}(V\Theta)-\frac{1}{Re_L Pr}\left(\frac{\partial^2 \Theta}{\partial X^2}+\frac{\partial^2 \Theta}{\partial Y^2}\right)=0 \tag{4}$$

The length, velocity, temperature and pressure scales selected to normalize the equations are L, u_w, $(T_w - T_\infty)$ and ρu_w^2, respectively. The above set of equations can be represented by a single equation of the form:

$$\frac{\partial}{\partial X}(U\phi)+\frac{\partial}{\partial Y}(V\phi)-\frac{\Gamma_\phi}{Re_L}\left(\frac{\partial^2 \phi}{\partial X^2}+\frac{\partial^2 \phi}{\partial Y^2}\right)=S_\phi \tag{5}$$

where ϕ is the general variable and stands for 1, U, V and Θ in Eqs. (1)–(4), respectively; Γ_ϕ is a dimensionless exchange coefficient whose values are 0, 1, 1 and $1/Pr$ in the above equations, respectively; and S_ϕ is a source term that represents the right-hand-side of the equations. This general form of transport equation facilitates the use of the same solution procedure for all equations.

2.2. Boundary conditions

With reference to Fig. 1, where the plate is drawn vertically upward from the slot at $x = 0$, the following boundary conditions are applied.

2.2.1. Plate surface

The plate is porous and continuously moving at which

$$u=u_w, \quad v=v_w \quad \text{and} \quad T=T_w \tag{6}$$

where u_w and T_w are constants. The transpired velocity v_w is given by

$$v_w = Du_w \tag{7a}$$

where D is a dimensionless suction/injection parameter. This parameter is used for specifying uniform suction/injection through the plate, i.e. for uniform v_w. Positive or negative D implies injection or suction, respectively.

For non-uniform suction/injection, v_w is given by

$$v_w = D_F v Re_x^{1/2}/x \tag{7b}$$

or

$$v_w = 3D_N v(Gr_x/4)^{1/4}/x \tag{7c}$$

where D_F and D_N are dimensionless suction/injection parameters used for forced and natural convection, respectively. The normal velocity at the surface v_w must vary along the plate as $x^{-1/2}$ according to Eq. (7b) to obtain similarity solutions for pure forced convection, Fox et al. [11]. For pure natural convection, v_w must vary as $x^{-1/4}$ accordingly to Eq. (7c) for similarity solutions to exist, Kays and Crawford [27]. Fortunately, in the present numerical model, there is no restriction to use either specification and whatever distribution of transpired velocity, as required by the practical situation, can be accommodated. Therefore, the distributions given by Eqs. (7b) and (7c) are used only to facilitate comparisons with solutions based on the similarity approach. For the more practical case of uniform suction or injection, Eq. (7a) is used throughout for which similarity solutions do not exist.

2.2.2. Extrusion die wall

The surface of the extrusion die, with the exception of the slot, represents an impervious and stationary wall at which

$$u=0, \quad v=0 \quad \text{and} \quad T=T_\infty \tag{8}$$

It was shown in [25,26] that this side wall has an effect in creating a flow re-circulation region outside the boundary layer as a result of fluid entrainment toward the moving plate. Therefore, the region close to the extrusion slot is strictly elliptic and the boundary layer approximations cannot be applied.

2.2.3. Free stream

The free stream boundary is located far away from the moving plate, therefore

$$u=0, \quad v=v_e, \quad T=T_\infty \quad \text{and} \quad p=p_\infty \tag{9}$$

This boundary is allowed to entrain fluid at velocity v_e and temperature T_∞. The velocity v_e is not known beforehand and is determined iteratively by the calculations. Its value depends upon the mass flow rate drawn outside the calculation domain by the viscous action of the moving plate and the mass flow rate due to suction or injection through the plate.

2.2.4. Outlet

The following conditions are applied at the outlet boundary:

$$\frac{\partial u}{\partial x}=0,\quad \frac{\partial v}{\partial x}=0,\quad \frac{\partial T}{\partial x}=0 \quad \text{and} \quad p=p_{\infty} \tag{10}$$

These approximate fully developed conditions and are quite adequate in the parabolic dominated flow region especially when the outlet is ensured to be located far downstream from the extrusion slot.

2.3. Numerical solution procedure

The numerical model uses a control-volume finite-difference method for discretizing the governing partial-differential equations, Eqs. (1)–(4), and is essentially the same as that used in [25,26]. The pressure field and velocities are determined via the well-known SIMPLE algorithm of Patankar and Spalding [28], with a slight difference in the way the finite-volume equations are solved. The 2/E/FIX computer program of Pun and Spalding [29] was modified and used to solve the present problem. The finite-volume equations are handled by this code on a line-by-line manner. Al-Sanea et al. [30] described and applied the line-by-line procedure in computing re-circulating flows with heat transfer. The scheme was found particularly beneficial for flows where relatively large parabolic or nearly parabolic regions exist along side the elliptic flow regions. The present moving plate problem with surface mass transfer falls into such a category where elliptic effects are dominant in the region close to the extrusion slot while far enough downstream the flow is predominantly parabolic.

The numerical results are checked to be substantially grid independent. This is achieved by obtaining solutions with an increasing number of grid nodes until a stage is reached where the solution exhibits negligible change with further increase in the number of nodes. The boundary layer thickness increases with distance downstream from the slot and is influenced by Re_L, Pr, B and D. Therefore, the locations of the free stream and outlet boundaries are checked by numerical experiments to be far enough not to influence the results in the region of interest. For example, the free stream boundary would be located at a distance of about 10% L which is greater than twice the maximum thickness of the boundary layer present at the very end of the plate for $Re_L = 10^4$, $Pr = 1$, $B = 10^{-2}$ and $D = 0$.

A non-uniform finite-volume grid is used with nodes closely spaced in regions with steep variation of flow properties; namely, near to the extrusion slot and the plate. A grid size of 100×50 nodes in the x- and y-directions, respectively, is normally employed. The grid step sizes, Δx and Δy, increase in the x- and y-directions with expansion factors of about 1.1 and 1.2, respectively.

Converged solutions are achieved when the changes in all variables, for all nodes, produced in successive iterations diminish and when the sums of the residual errors in the finite-volume equations are reduced to a small value. Typical converged results are obtained after about 700 iterations starting from uniform initial fields; a near optimum relaxation factor in the range 0.2–0.5 is applied for the variables. Considerably larger number of iterations is needed for the pure natural convection calculations and for those physical situations dominated by natural convection. The calculations require about 1×10^{-6} s of CPU time per iteration for each variable for each grid node on a 700-megahertz Intel Pentium III microcomputer.

3. Results and discussion

The heat transfer and friction characteristics are investigated for different Prandtl numbers ($0.1 \leqslant Pr \leqslant 10$). Only buoyancy-assisting flows are considered and a wide range of the buoyancy force parameter is covered ($10^{-4} \leqslant B \leqslant 1$). The suction/injection parameter is varied over the range ($-0.10 \leqslant D \leqslant 0.05$).

3.1. Numerical model validation

The forced convection problem was studied in detail in both the non-similar and self-similar regions by Al-Sanea and Ali [25], in which the numerical model was validated against the similarity method solutions and previously published data. The entire forced, mixed and natural convection regions were analyzed by Al-Sanea [26], in which comparisons with published experimental measurements and solutions by others in the pure forced and pure natural convection regions were made. In the mixed convection region, the numerical results were compared with finite difference solutions of the boundary layer equations showing excellent agreement. In the present study, further validation is carried out since the model is extended to deal with both buoyancy effects in the flow and mass transfer at the surface.

Fig. 2 depicts the variation of $Nu_x Re_x^{-1/2}$ with the dimensionless distance along the plate in terms of the local Richardson number (Ri_x). The figure shows comparisons between the present finite-volume elliptic solutions and the boundary layer solutions of Ali and Al-Yousef [18] by using the fourth-order Runge–Kutta method for $Pr = 0.72$ and $D_F = -0.6$, 0 and 0.6. Comparison is also made with the finite-difference solutions of the boundary layer equations by Moutsoglou and Chen [20] for $D_F = 0$ (no suction or injection) that extend over a small range in the mixed convection region. The current results are presented for $B = 10^{-4}$; however, for $D_F = -0.6$, results are also presented for $B = 10^{-3}$ and 10^{-2} in order to investigate the effect of B. The

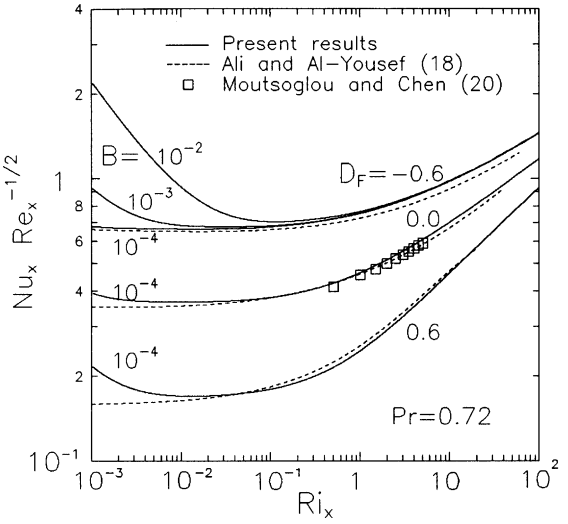

Fig. 2. Nusselt number variation with Richardson number showing comparison with boundary layer solutions [18,20] for $Pr = 0.72$ and different B and D_F; non-uniform suction/injection.

parameter D_F, defined by Eq. (7b) for non-uniform suction or injection, is used in [18] to obtain local similarity solutions for the mixed convection problem.

At low Ri_x (close to the extrusion slot), where the stream-wise diffusion is important and the full Navier–Stokes equations need to be solved, the present predictions show a sharp decrease in $Nu_x Re_x^{-1/2}$ with increasing Ri_x. On the other hand, the boundary layer solutions do not give this behavior but lead asymptotically to the corresponding pure forced convection values as $Ri_x \to 0$ [25]. It is noted that the curves for $D_F = -0.6$ and different values of B meet and collapse onto a single line, as the stream-wise diffusion diminishes with increasing Ri_x, and both the elliptic and boundary layer solutions give practically the same results. This single line approaches asymptotically the pure natural convection results at large Ri_x as will be seen later. The figure also reveals that the heat transfer rate increases with B and suction and decreases with injection. The agreement between the present predictions and those reported in [18,20] is excellent.

The numerical model is also validated under pure natural convection conditions. This is affected by setting $u_w = 0$ in which the external inertia forces vanish and the flow would be driven only by buoyancy forces and mass transfer through the stationary plate. It is emphasized that the suction/injection parameter is now D_N as defined by Eq. (7c) and is used to obtain similarity solutions for the purpose of comparison. Under these conditions, the local Nusselt number is a function of Pr, D_N and Gr_x. Fig. 3(a) depicts the variation of $Nu_x Gr_x^{-1/4}$ with Gr_x for $Pr = 0.73$ and different D_N. At large Gr_x and for a given Pr, $Nu_x Gr_x^{-1/4}$ is a function of D_N only. This is true in the self-similar region where the stream-wise diffusion is very small and can be neglected and, therefore, the boundary layer approximations are valid. However, at small Gr_x and for given Pr and D_N, $Nu_x Gr_x^{-1/4}$ is not a constant but increases sharply with decreasing Gr_x in the non-similar region as the stream-wise diffusion increases.

At low enough Gr_x, viscous forces dominate over the buoyancy forces and the energy equation reduces to a pure conduction equation in which both Pr and D_N have no relevance. The results in Fig. 3(a) show this behavior in which $Nu_x Gr_x^{-1/4}$ becomes independent of D_N at low Gr_x. At the other extreme of large Gr_x, $Nu_x Gr_x^{-1/4}$ reaches asymptotically the self-similar values for each D_N as indicated by the long-dashed horizontal straight lines. These self-similar asymptotic values reported by Eich-

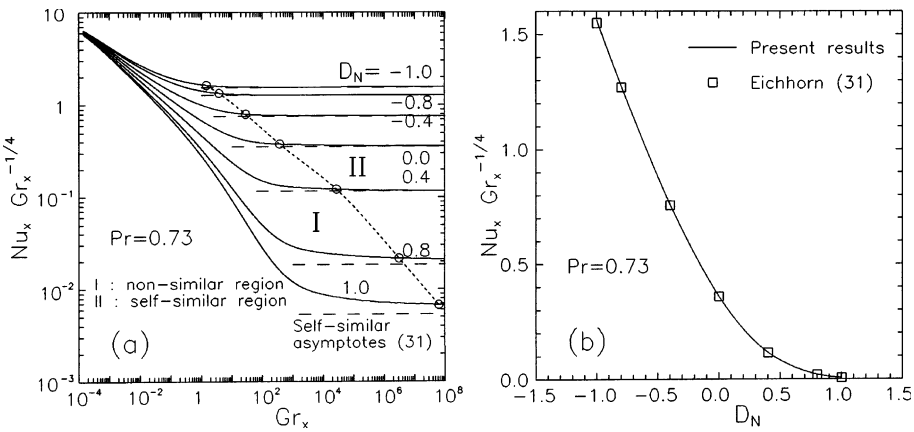

Fig. 3. Pure natural-convection heat transfer results showing comparison with asymptotic values [31] for $Pr = 0.73$ and different D_N: (a) Nusselt number variation with Grashof number, and (b) Nusselt number variation with D_N at large Gr_x; non-uniform suction/injection.

horn [31] agree perfectly well with the present finite-volume results at large Gr_x as shown in Fig. 3(b). The results also show that the heat transfer rate increases with suction and decreases with injection as expected.

The short dashed line drawn in Fig. 3(a) distinguishes the non-similar natural convection region to the left (region I) from the self-similar region to the right (region II) by connecting the critical values of Grashof number ($Gr_{x,c}$) for different D_N. These critical values are calculated as follows: $Gr_{x,c}$ is obtained for a given D_N by calculating Gr_x at which $Nu_x Gr_x^{-1/4}$ deviates by 5% from its self-similar asymptotic value. The results show that $Gr_{x,c}$ decreases with decreasing injection and increasing suction.

3.2. Heat transfer characteristics for uniform suction

Representative mixed-convection heat transfer characteristics along the plate are shown in Fig. 4(a) and (b) for $Pr = 1$, $B = 10^{-2}$ and $D = -0.02$ (solid lines). The parameter D is defined by Eq. (7a) for the case of uniform suction or injection. Heat transfer results are also shown for each convection mode acting alone in the absence of the other mode (dashed lines). The computer program is, thus, run three times: a first time under mixed convection conditions to produce the mixed convection results, a second time with the buoyancy term "switched off" to produce the pure forced convection results, and a third time with the buoyancy term on but with a stationary plate ($u_w = 0$) to produce the pure natural convection results. For the latter case, $u_w = 0$ is used only to suppress the inertia forces of the plate but not in the definition of v_w according to Eq. (7a). For the pure natural convection case, the suction/injection parameter (D) is based on a finite (non-zero) value of u_w. This value of u_w is the same as that used in the pure forced and mixed convection cases in order to compare the heat transfer rates of the different convection modes.

It is noted that the results plotted in Fig. 4(a) are in terms of the heat flux variation with distance along the surface. These dimensional variables are very specific in nature and their absolute values depend upon the very specific values assigned to the fluid properties and T_w, T_∞, β, u_w, etc. Therefore, and in order to generalize these results, appropriate normalization is needed. However, the different convection modes considered in the present problem require some form of transformation. Normally, Re_x, Ri_x and Gr_x would be the appropriate dimensionless numbers representing the dimensionless distance along the surface for the pure forced, mixed and pure natural convection modes, respectively. Any particular location x on the surface corresponds to genuine values of Re_x, Ri_x and Gr_x through the definitions of these numbers. Hence, in order to present all results in dimensionless form on one plot, a decision is made to choose Ri_x to represent a convenient dimensionless distance along the surface as is done in Fig. 4(b). It is also noted that the local heat flux is represented more generally in terms of the local Nusselt number divided by square root of the local Reynolds number. Besides, the natural convection results in terms of $Nu_x Gr_x^{-1/4}$ are transformed into the form of forced and mixed convection results in terms of $Nu_x Re_x^{-1/2}$ through the definition of the local Richardson number viz.:

$$Nu_x Re_x^{-1/2} = Nu_x Gr_x^{-1/4} Ri_x^{1/4} \tag{11}$$

Accordingly, a suitable criterion to delineate the forced, mixed and natural convection regimes can be used as will be outlined next.

It is interesting to note that $Nu_x Re_x^{-1/2}$ for the pure forced convection is equal to that for the pure natural convection at $Ri_x \approx 1$ (see Fig. 4(b)), where the two

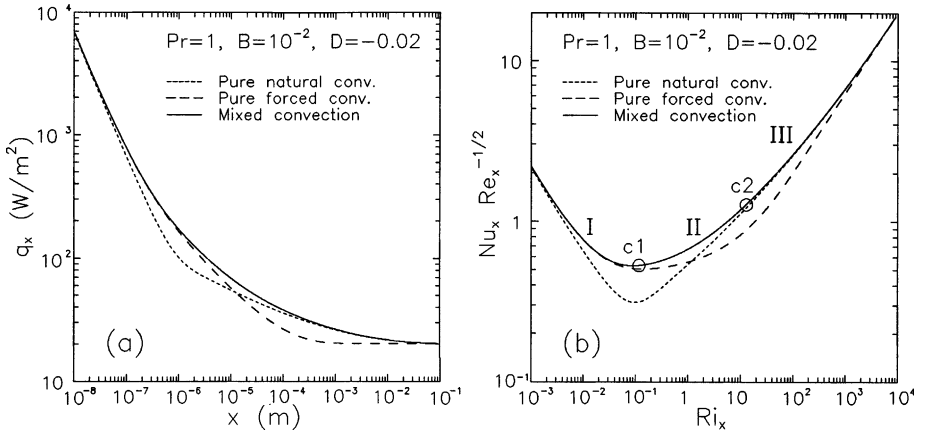

Fig. 4. Heat transfer rate variation along the surface showing results of pure natural, pure forced and mixed convection modes for $Pr = 1$, $B = 10^{-2}$ and $D = -0.02$: (a) heat flux variation with distance, and (b) Nusselt number variation with Richardson number.

dashed lines intersect, at which the heat transfer rate is the same from either mode. For Ri_x less than about 1, the pure forced-convection heat transfer rate is greater than that of the pure natural convection. For Ri_x greater than about 1, the opposite is true due to heat transfer enhancement caused by increasing buoyancy forces. It is also interesting to note how $Nu_xRe_x^{-1/2}$ for the mixed convection deviates (increases) gradually from the pure forced convection results at $Ri_x \approx 0.1$ and approaches asymptotically the natural convection results at $Ri_x \approx 10$. Besides, the forced convection results reach asymptotically both the natural and mixed convection results at $Ri_x > 10^3$ due to the suction effect.

Another interesting feature of the results in Fig. 4(b) is that $Nu_xRe_x^{-1/2}$ is the same for any convection mode at low Ri_x ($Ri_x < 3 \times 10^{-3}$). This is attributed to the fact that diffusion dominates at low Ri_x and, hence, the temperature field is not affected by the velocity field. Therefore, the heat transfer rate at the plate surface becomes independent of the convection mode.

A method used by previous investigators to delineate the mixed convection regime for the Blasius boundary-layer problem is used in the present study to delineate the convection regimes for the moving plate problem. This is based on the "5% criterion", i.e. on the heat transfer enhancement due to mixed convection over either of the pure forced or pure natural convection results. Therefore, a 5% increase in $Nu_xRe_x^{-1/2}$ over that of pure forced convection would mark the critical Richardson number ($Ri_{x,c1}$) that distinguishes the pure forced convection regime from the mixed convection regime. Similarly, a 5% increase in $Nu_xRe_x^{-1/2}$ over that of pure natural convection would mark $Ri_{x,c2}$ that distinguishes the pure natural convection regime from the mixed convection regime. A demonstration of this criterion is shown in Fig. 4(b). Two circles, $c1$ and $c2$, are marked on the mixed convection line corresponding to $Ri_{x,c1}$ and $Ri_{x,c2}$, respectively. Region I represents the forced-convection dominated region, region II represents the mixed convection region and region III represents the natural-convection dominated region. This procedure is applied for different Pr, B and D. Tables and maps showing the various convection regimes are given later.

With regard to the execution of the 5% criterion, it was found convenient to adopt the following procedure. First, multiply values of $Nu_xRe_x^{-1/2}$ for the pure forced convection case by 1.05 and then plot these results versus Ri_x along with $Nu_xRe_x^{-1/2}$ variation with Ri_x for the mixed convection case. The point of intersection of these two curves would mark point $c1$; Ri_x that corresponds to this point would be $Ri_{x,c1}$. A similar procedure is done for point $c2$ and $Ri_{x,c2}$. Critical Richardson numbers evaluated by using the 5% criterion are compared with available results by others in Section 3.6.

Referring back to the results at large Ri_x, it was already noted that all the convection modes give the same heat transfer rate (see Fig. 4(a) and (b)). This interesting behavior is attributed to the fact that under the condition of uniform suction and at locations far downstream from the slot, suction dominates momentum transfer in the boundary layer and an asymptotic state is reached where the boundary layer thickness becomes constant. Therefore, the velocity and temperature profiles become independent of the stream-wise location as will be presented in Section 3.3. Under these conditions, the energy equation is simplified and can be solved analytically to give the following exact solution:

$$\theta = \exp(v_w y/\alpha) \tag{12}$$

It is noted that v_w must be negative (suction only), otherwise θ would be unbounded at large y. Further analysis yields Stanton number (St) as:

$$St = Nu_L/(Re_L Pr) = h/(\rho u_w c_p) = -v_w/u_w \tag{13}$$

Therefore, at the asymptotic state, the Stanton number is a constant ($= -D$) and the heat transfer rate is, hence, independent of the convection mode.

Similarly, under asymptotic state conditions, the stream-wise momentum equation is simplified and exact analytic solutions can be derived for the velocity profiles and the friction coefficient as:

$$u = [u_w - \{g\beta(T_w - T_\infty)y\}/v_w]\exp(v_w y/\nu) \tag{14}$$

$$C_f = [\rho u_w v_w - \{\mu g\beta(T_w - T_\infty)\}/v_w]/(0.5\rho u_w^2) \tag{15}$$

Therefore, at the asymptotic suction state, the stream-wise velocity is a function of y only and the friction coefficient attains a constant value. Eqs. (14) and (15) are the solutions affected for $Pr = 1$.

The mixed-convection heat transfer results in terms of the Stanton number (St_x) variation with Ri_x are presented in Fig. 5(a) for $Pr = 1$, $B = 10^{-2}$ and different values of D. The long-dashed horizontal straight lines represent the exact asymptotic suction solutions given by Eq. (13). It is noted that the case with no suction ($D = 0$) does not yield an asymptotic state. The short-dashed line drawn on the figure distinguishes the asymptotic suction region (region II located to the right) from the initial region (region I located to the left). This line connects the critical values of Richardson number ($Ri_{x,c3}$) for different values of D. These critical values are calculated as follows: $Ri_{x,c3}$ is obtained for a given D by calculating Ri_x at which St_x deviates by 5% from its exact asymptotic suction value. The results show that $Ri_{x,c3}$, i.e. the initial length along the surface before the asymptotic state is reached, increases with decreasing suction. Also, for a given D, $Ri_{x,c3}$ is much greater than $Ri_{x,c2}$. Hence, the asymptotic state is reached at a location well into the natural-convection dominated region. For example, Fig. 5(a) gives $Ri_{x,c3} \approx 900$ for $D = -0.02$; this is compared with $Ri_{x,c2} \approx 10$ in Fig. 4(b).

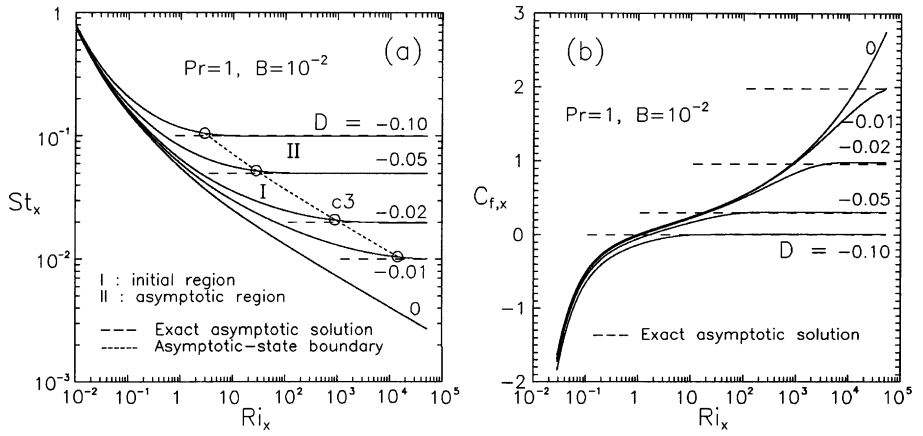

Fig. 5. Stanton number and skin-friction coefficient variations along the surface showing comparison with exact asymptotic solutions for $Pr = 1$, $B = 10^{-2}$ and different D: (a) St_x versus Richardson number, and (b) $C_{f,x}$ versus Richardson number.

The corresponding results in terms of the friction coefficient ($C_{f,x}$) variation with Ri_x are presented in Fig. 5(b). The dashed horizontal lines represent the exact asymptotic suction solutions given by Eq. (15). The results show that the initial length along the surface required to reach the asymptotic state is longer for the hydrodynamic characteristics than the thermal characteristics (cf. Fig. 5(a) and (b)). This is especially true at weaker suction; indeed, for $D = -0.01$, the asymptotic state is just about reached for $C_{f,x}$ at $Ri_x \approx 4 \times 10^4$; for St_x, the asymptotic state is reached at $Ri_x < 2 \times 10^4$. More details regarding this point will be given in the next section. Finally, the agreement between the exact asymptotic suction values and the finite-volume results for both St_x and $C_{f,x}$ is excellent. This gives further validation to the numerical model.

3.3. Temperature and velocity distributions

Representative dimensionless temperature profiles at different stream-wise locations given by Ri_x are displayed in Fig. 6(a)–(d) for $Pr = 1$, $B = 10^{-2}$ and different values of D. The exact asymptotic suction profiles given by Eq. (12) are also shown for comparison at large Ri_x. The profiles extend over a wide range of Ri_x starting from the forced-convection dominated region, covering the entire mixed convection region, and ending well into the natural-convection dominated region. It is clear that the thermal boundary-layer thickness increases with Ri_x throughout the initial length. The temperature gradients at the surface ($y = 0$) and, therefore, St_x decrease with increasing Ri_x before reaching a constant asymptotic value as already shown in Fig. 5(a). It is noted that the transverse dimensionless distance, given by $-v_w y/\alpha$, is self adjusted to account for the effect of varying D through its influence on v_w and hence gives the same asymptotic suction profile regardless of the value of D. However, the profiles are different throughout the initial length.

The profiles are given at nine stream-wise locations; namely, $Ri_x = 10^{-2}$, 0.1, 1, 10, 10^2, 10^3, 10^4, 2×10^4 and 3×10^4. Fig. 6(a), for $D = -0.01$, shows that the last two profiles (at $Ri_x = 2 \times 10^4$ and 3×10^4) collapse practically on one line and are close to the profile at $Ri_x = 10^4$. Therefore, the asymptotic suction state is reached somewhere in the range $10^4 < Ri_x < 2 \times 10^4$. This is consistent with the results shown in Fig. 5(a) where $Ri_{x,c3}$ for $D = -0.01$ is calculated at about 1.4×10^4. The thermal boundary layer approaches a constant thickness at $Ri_x > 1.4 \times 10^4$. Fig. 6(b), for $D = -0.02$, shows that the last three profiles given by $Ri_x = 10^4$, 2×10^4 and 3×10^4 collapse on a single line and are close to the profile at $Ri_x = 10^3$. This is also consistent with the results in Fig. 5(a) where $Ri_{x,c3}$ is calculated at about 900. Again, the boundary layer approaches a constant thickness at $Ri_x > 900$. Similar remarks can be made on the results in Fig. 6(c) and (d) for $D = -0.05$ and -0.10 where $Ri_{x,c3}$ are calculated at about 30 and 3, respectively. As to the agreement between the finite-volume results at large Ri_x and the exact asymptotic temperature profiles, this may be described as excellent.

The corresponding velocity profiles are presented in Fig. 7(a)–(d). The stream-wise velocity component is normalized by the plate velocity ($U = u/u_w$) and the transverse distance y is normalized by the displacement thickness ($-v/v_w$). Compared to the temperature profiles in Fig. 6(a)–(d), it is seen that the initial lengths needed to reach the asymptotic suction state are longer for the velocity compared to those needed for the temperature. Indeed, the velocity profiles at $Ri_x = 2 \times 10^4$ and 3×10^4 in Fig. 7(a) fall little short of the asymptotic suction profile for $D = -0.01$. This is consistent with the results shown earlier in Fig. 5(b). Besides, the initial length decreases with increasing suction. For example, for

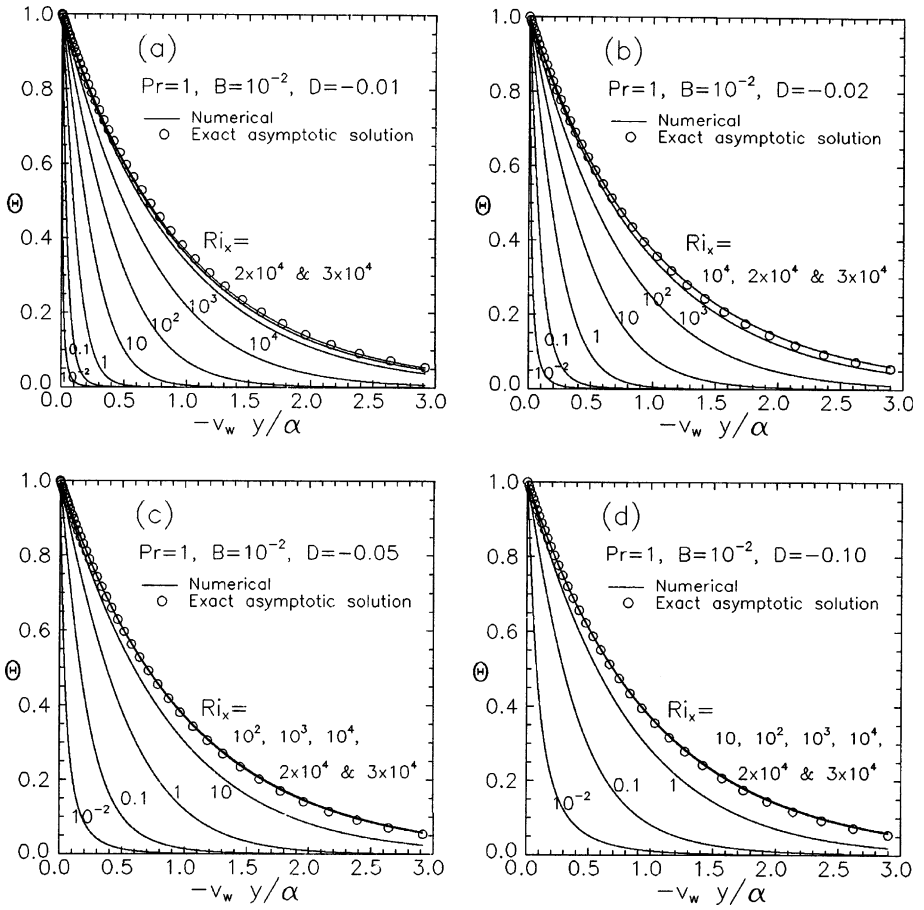

Fig. 6. Dimensionless temperature profiles at different Richardson numbers for $Pr = 1$ and $B = 10^{-2}$: (a) $D = -0.01$, (b) $D = -0.02$, (c) $D = -0.05$, and (d) $D = -0.10$.

$D = -0.10$, all velocity profiles collapse on a single line for Ri_x greater than about 10, as shown in Fig. 7(d). The agreement between the numerical results at large Ri_x and the exact asymptotic velocity profiles given by Eq. (14) is very good. For the results presented in Fig. 7(a) (weak suction), the numerical calculations need to be carried out further downstream ($Ri_x > 3 \times 10^4$) so that the velocity profiles approach the asymptotic state.

It is noted that $U = 1$ at the plate surface ($y = 0$) and approaches zero (the stagnant ambient condition) at large y. There is, in general, velocity overshoot ($U > 1$) where the fluid velocity exceeds the plate velocity. This velocity overshoot is due to the buoyancy forces which increase with Ri_x. The maximum velocity in the boundary layer is calculated at about 35 times that of the moving plate at $Ri_x = 3 \times 10^4$, as shown in Fig. 7(a) for $D = -0.01$. The location of the maximum velocity shifts away from the plate surface with increasing Ri_x. The magnitude of the velocity overshoot decreases with increasing suction and disappears from all profiles for $D = -0.10$, as shown in Fig. 7(d). It is also interesting to note that the velocity gradient at the surface changes sign due to the velocity overshoot. This has a corresponding effect on the skin friction coefficient presented in Fig. 5(b) where $C_{f,x}$ changes from negative to positive at $Ri_x \approx 1$ to 2. For $D = -0.1$ and Ri_x greater than about 5, $C_{f,x}$ is practically zero. This suggests that the velocity gradients at the surface are very close to zero, i.e. the plate and adjacent fluid move at about the same speed. The blunt shape of the velocity profiles at $y = 0$ shown for $Ri_x = 10$ in Fig. 7(d) supports this behavior.

Another interesting feature of the velocity profiles is the presence of negative values at low Ri_x (close to the extrusion slot). The negative velocities are more clearly seen in Fig. 7(c) and (d) due to the magnified y-axis. This indicates the presence of a reverse flow region outside the boundary layer as a consequence of an adverse pressure gradient directed toward the slot. The adverse pressure gradient is created by the action of the moving plate, fluid entrainment toward the plate surface and the effect of the side wall (extrusion die). The re-circulation region disappears further downstream with increasing Ri_x.

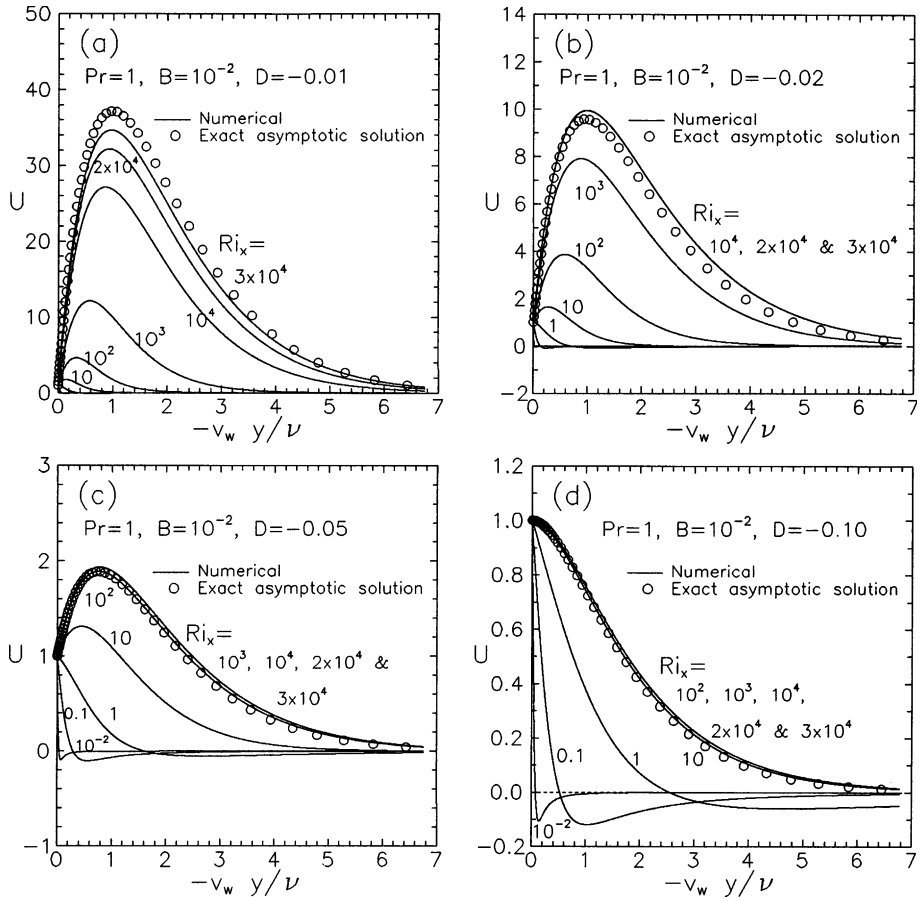

Fig. 7. Dimensionless velocity profiles at different Richardson numbers for $Pr = 1$ and $B = 10^{-2}$: (a) $D = -0.01$, (b) $D = -0.02$, (c) $D = -0.05$, and (d) $D = -0.10$.

3.4. Parametric study

The thermal characteristics in terms of $Nu_x Re_x^{-1/2}$ variations with Ri_x are presented in Figs. 8–10 showing the effects of varying Pr, B and D. Two dashed lines are drawn on each figure to distinguish between the forced-convection dominated region (region I), the mixed convection region (region II) and the natural-convection dominated region (region III). These dashed lines connect the values of $Ri_{x,c1}$ (to distinguish region I from II) and $Ri_{x,c2}$ (to distinguish region II from III). Both $Ri_{x,c1}$ and $Ri_{x,c2}$ are determined by applying the 5% criterion explained earlier.

Fig. 8(a)–(c) present the results for $B = 10^{-4}$ and $Pr = 0.1$, 1 and 10, respectively, with D as a varying parameter in each figure. In general, $Nu_x Re_x^{-1/2}$ decreases with increasing Ri_x throughout the forced-convection dominated region. In the mixed convection region that follows, $Nu_x Re_x^{-1/2}$ generally levels off and then increases with Ri_x (except when there is a strong injection) as heat transfer enhancement takes place due to increasing buoyancy forces. In the natural-convection dominated region, $Nu_x Re_x^{-1/2}$ increases further with Ri_x for suction, however, it decreases with increasing Ri_x for injection. For a given Ri_x, $Nu_x Re_x^{-1/2}$ increases with suction and decreases with injection. Also, the effect of suction and injection increases with increasing Ri_x.

As for the influence of Prandtl number, the heat transfer rate increases with Pr as shown in Fig. 8(a)–(c). It is noted that the heat transfer results become more sensitive to D as Pr increases. Also, the forced-convection dominated region extends further downstream with increasing Pr; the values of $Ri_{x,c1}$ are about 0.006, 0.13 and 1.5 for $Pr = 0.1$, 1 and 10, respectively. These values are affected slightly by D. On the other hand, the mixed convection region extends downstream (i.e. $Ri_{x,c2}$ increases) with decreasing suction or increasing injection and is much more sensitive to D. It is noted that the mixed convection region may extend to very low Ri_x as the suction parameter and Prandtl number increase, see Fig. 8(b) and (c). This is due to the reason that, for these conditions, the heat transfer rates calculated under the

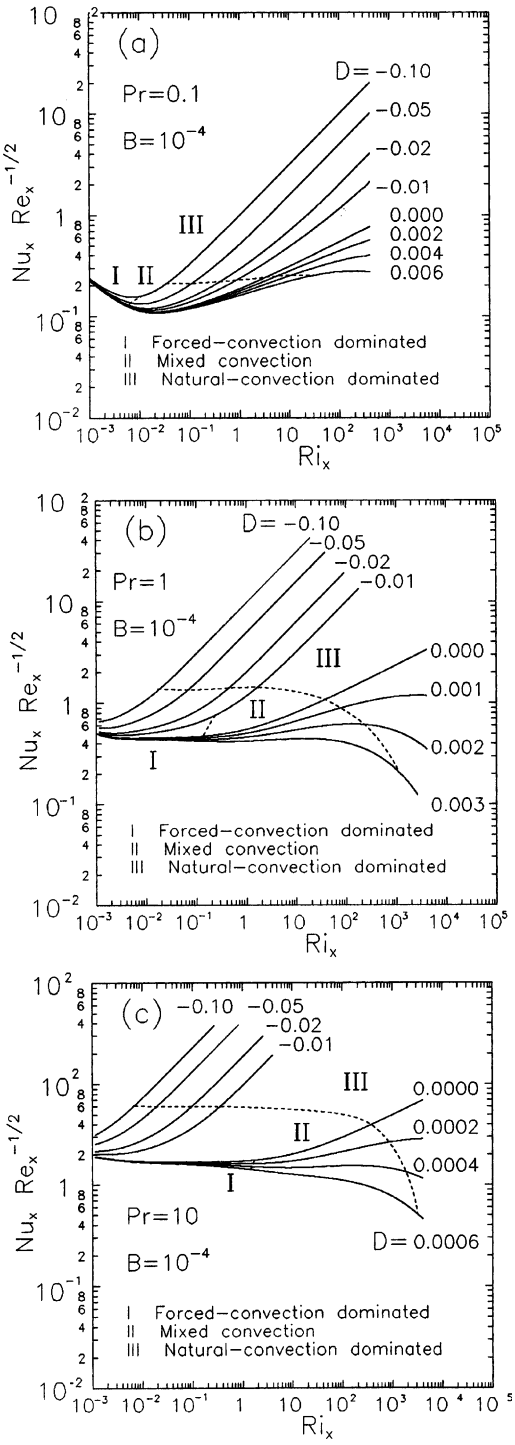

Fig. 8. Nusselt number variation with Richardson number for $B = 10^{-4}$ and different D: (a) $Pr = 0.1$, (b) $Pr = 1$, and (c) $Pr = 10$.

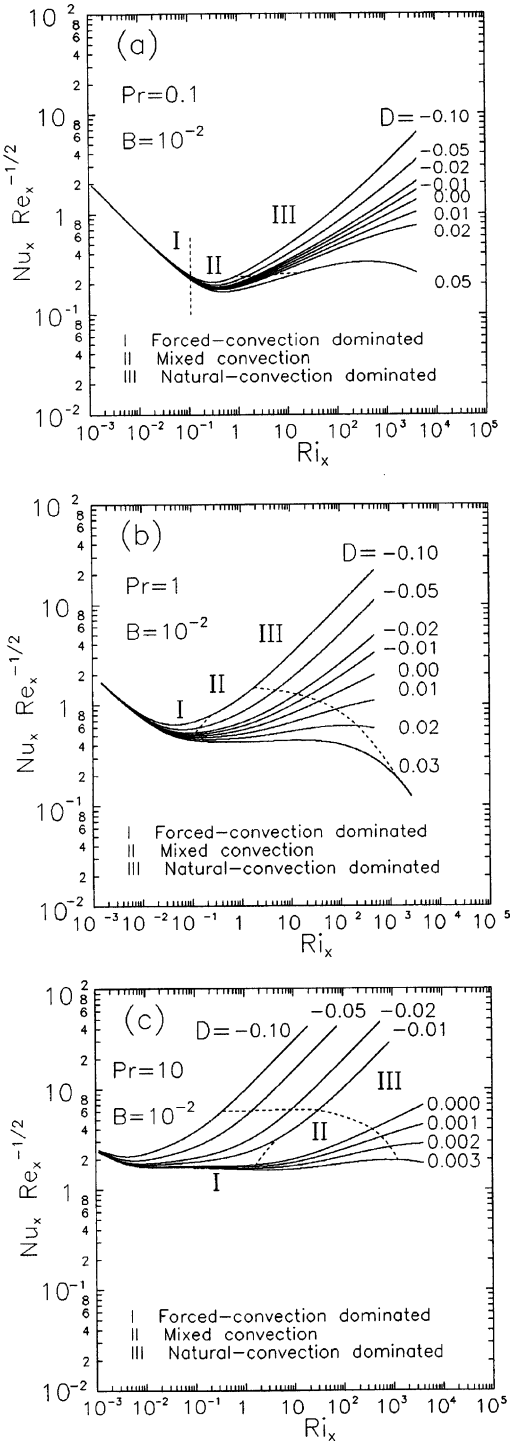

Fig. 9. Nusselt number variation with Richardson number for $B = 10^{-2}$ and different D: (a) $Pr = 0.1$, (b) $Pr = 1$, and (c) $Pr = 10$.

pure forced convection conditions are only marginally lower than those calculated under the mixed convection conditions so that the 5% criterion overshoots the mixed convection results and $Ri_{x,c1}$ cannot be found. Therefore,

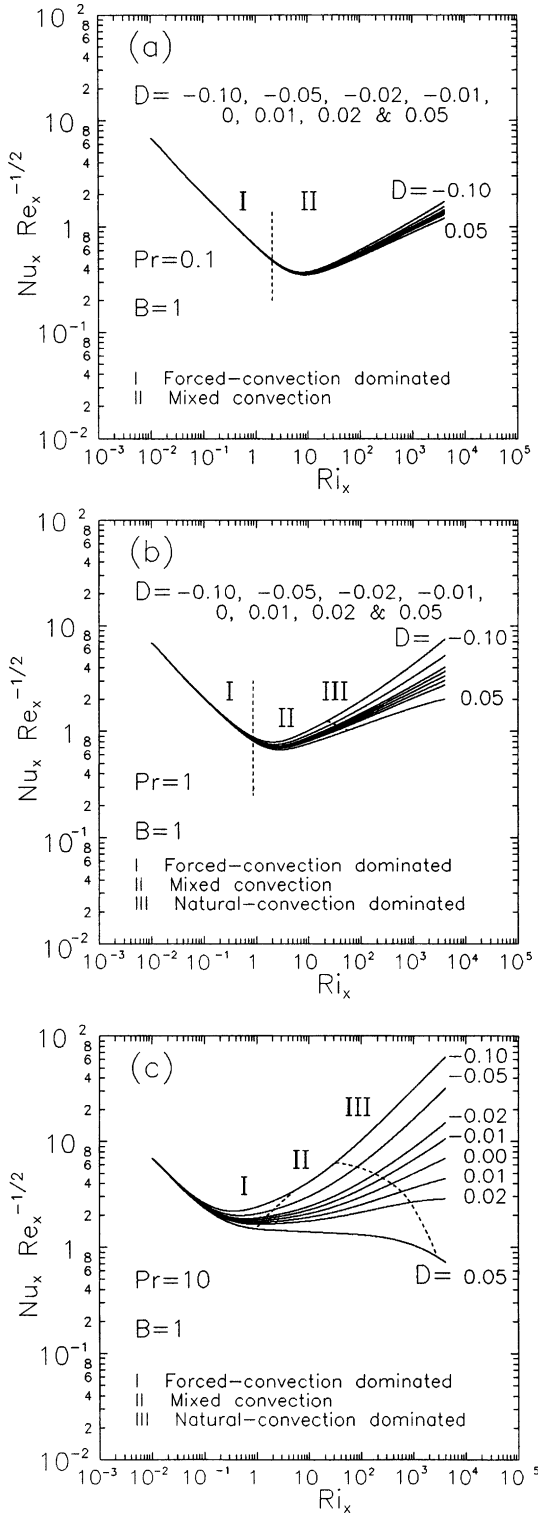

Fig. 10. Nusselt number variation with Richardson number for $B = 1$ and different D: (a) $Pr = 0.1$, (b) $Pr = 1$, and (c) $Pr = 10$.

the forced and mixed convection regions cannot be separated. Values of Ri_x for the various convection regimes are summarized in Table 1. The two critical Richardson numbers ($Ri_{x,c1}$ and $Ri_{x,c2}$) are the lower and upper limits in the mixed convection range.

The corresponding results for different values of the buoyancy force parameter are shown in Fig. 9(a)–(c) for $B = 10^{-2}$, and in Fig. 10(a)–(c) for $B = 1$. Similar trends of variations are obtained for the effects of Pr and D as those already discussed for $B = 10^{-4}$ in Fig. 8(a)–(c). However, as B increases the sensitivity of the heat transfer results to D decreases especially at low values of Ri_x and Pr. For example, the curves for different D shown in Fig. 10(a) for $Pr = 0.1$ and $B = 1$ collapse on a single line in the forced-convection dominated region and occupy a relatively very narrow band in the mixed convection region. This is attributed to two factors; firstly, the thermal boundary-layer thickness for $Pr = 0.1$ is much thicker compared to those for $Pr = 1$ and 10 and, consequently, suction or injection at the plate surface becomes relatively less effective. Secondly, as B increases, the buoyancy forces increase which overshadow the effect of D. It is also noted that, in general, the forced-convection dominated region extends further downstream with increasing B.

For the parameters given in Fig. 10(a), the heat transfer rates calculated under the mixed convection conditions are only marginally higher than those calculated under the pure natural convection conditions so that the 5% criterion cannot be applied and $Ri_{x,c2}$ cannot be found. Therefore, the mixed and natural convection regimes cannot be separated. Under such conditions, one may regard that the mixed convection regime to extend to very large Ri_x.

Values of Ri_x for the various convection regimes are summarized in Tables 2 and 3 for $B = 10^{-2}$ and 1, respectively.

The corresponding results for the skin-friction coefficient variation with Ri_x are presented in Figs. 11 and 12 for different Pr, B and D. The friction coefficient and, hence, the shear stress at the surface are negative when the plate velocity is greater than the adjacent fluid velocity. The positive friction coefficient indicates the opposite due to velocity overshoot caused by the buoyancy effect at large Ri_x. The zero shear stress does not imply boundary layer separation but corresponds to equal plate and adjacent fluid velocities.

Fig. 11(a)–(c) present the results for $B = 10^{-2}$ and $Pr = 0.1$, 1 and 10, respectively. It is noted that the locations of the vanishing shear stress at the plate move downstream with increasing Pr. Also, as the suction and Pr increase, the shear stress remains negative throughout which indicates the absence of velocity overshoot. This is due to the combined effects of suction and thinning of the thermal boundary layer (due to increasing Pr) which reduce the stream-wise velocity and also reduce the

Table 1
Range of Richardson number (Ri_x) for the various convection regimes showing the effect of Pr and D for $B = 10^{-4}$

Pr	D	Forced convection	Mixed convection	Natural convection
0.1	−0.10	$Ri_x < 0.012$	$0.012 \leqslant Ri_x \leqslant 0.034$	$Ri_x > 0.034$
0.1	−0.05	$Ri_x < 0.007$	$0.007 \leqslant Ri_x \leqslant 0.109$	$Ri_x > 0.109$
0.1	−0.02	$Ri_x < 0.006$	$0.006 \leqslant Ri_x \leqslant 0.397$	$Ri_x > 0.397$
0.1	−0.01	$Ri_x < 0.006$	$0.006 \leqslant Ri_x \leqslant 0.840$	$Ri_x > 0.840$
0.1	0.00	$Ri_x < 0.006$	$0.006 \leqslant Ri_x \leqslant 3.34$	$Ri_x > 3.34$
0.1	0.002	$Ri_x < 0.006$	$0.006 \leqslant Ri_x \leqslant 5.59$	$Ri_x > 5.59$
0.1	0.004	$Ri_x < 0.006$	$0.006 \leqslant Ri_x \leqslant 10.8$	$Ri_x > 10.8$
0.1	0.006	$Ri_x < 0.006$	$0.006 \leqslant Ri_x \leqslant 32.4$	$Ri_x > 32.4$
1.0	−0.10	$Ri_x < *$	$* \leqslant Ri_x \leqslant 0.018$	$Ri_x > 0.018$
1.0	−0.05	$Ri_x < *$	$* \leqslant Ri_x \leqslant 0.065$	$Ri_x > 0.065$
1.0	−0.02	$Ri_x < *$	$* \leqslant Ri_x \leqslant 0.440$	$Ri_x > 0.440$
1.0	−0.01	$Ri_x < 0.241$	$0.241 \leqslant Ri_x \leqslant 1.63$	$Ri_x > 1.63$
1.0	0.00	$Ri_x < 0.136$	$0.136 \leqslant Ri_x \leqslant 37$	$Ri_x > 37$
1.0	0.001	$Ri_x < 0.131$	$0.131 \leqslant Ri_x \leqslant 76$	$Ri_x > 76$
1.0	0.002	$Ri_x < 0.127$	$0.127 \leqslant Ri_x \leqslant 228$	$Ri_x > 228$
1.0	0.003	$Ri_x < 0.125$	$0.125 \leqslant Ri_x \leqslant 1102$	$Ri_x > 1102$
10	−0.10	$Ri_x < *$	$* \leqslant Ri_x \leqslant 0.004$	$Ri_x > 0.004$
10	−0.05	$Ri_x < *$	$* \leqslant Ri_x \leqslant 0.014$	$Ri_x > 0.014$
10	−0.02	$Ri_x < *$	$* \leqslant Ri_x \leqslant 0.083$	$Ri_x > 0.083$
10	−0.01	$Ri_x < *$	$* \leqslant Ri_x \leqslant 0.337$	$Ri_x > 0.337$
10	0.00	$Ri_x < 1.73$	$1.73 \leqslant Ri_x \leqslant 374$	$Ri_x > 374$
10	0.0002	$Ri_x < 1.63$	$1.63 \leqslant Ri_x \leqslant 845$	$Ri_x > 845$
10	0.0004	$Ri_x < 1.53$	$1.53 \leqslant Ri_x \leqslant 1850$	$Ri_x > 1850$
10	0.0006	$Ri_x < 1.45$	$1.45 \leqslant Ri_x \leqslant 3200$	$Ri_x > 3200$

$*Ri_{x,c1}$ could not be obtained since the 5% criterion overshot the mixed convection results throughout the whole region.

buoyancy forces. It is interesting to note that the friction coefficient is less sensitive to D at low Ri_x. Also, the effect of Pr on the friction coefficient for a given D diminishes for $Ri_x < 0.1$ since forced convection becomes dominant and, hence, the hydrodynamics become independent of the heat transfer.

The results presented in Fig. 11(a) for $Pr = 0.1$ show that suction gives a higher friction coefficient than injection except over a small region at $1 < Ri_x < 2$. All curves for different D cross each other and, therefore, give approximately the same friction coefficient at $2 < Ri_x < 3$. This trend is not seen in Fig. 11(b) and (c) (for $Pr = 1$ and 10) where at $Ri_x > 5$ and when there is a velocity overshoot ($C_{f,x} > 0$), suction acts to decrease the friction coefficient while injection acts to increase it. On the other hand, at low Ri_x, the exact opposite behavior takes place where suction acts to increase the friction coefficient while injection acts to decrease it as expected in the forced-convection dominated region.

Fig. 12(a) and (b) present the skin-friction coefficient variations for $B = 10^{-4}$ and 1, respectively, and for $Pr = 1$. These results are complemented by those already presented in Fig. 11(b) for $B = 10^{-2}$. It is noted that as B increases, the friction coefficient becomes less sensitive to D. Indeed, for the range of parameters shown in Fig. 12(b), all the curves for different values of D effectively collapse on a single line.

3.5. Convection regimes maps

Maps for delineating the forced, mixed and natural convection regimes are presented as a function of Reynolds and Grashof numbers for $Pr = 1$, $B = 10^{-2}$ and for $D = -0.10$, -0.02, -0.01, 0, 0.01 and 0.02 in Fig. 13(a)–(f), respectively. The mixed convection regime is bound by the boundaries shown in the figures which are determined from $Ri_{x,c1}$ and $Ri_{x,c2}$. The convection map for $D = -0.10$ is characterized by a relatively narrow mixed convection regime as shown in Fig. 13(a). The mixed convection regime widens as suction is reduced and injection is increased. It is noted that the forced convection boundary, and hence $Ri_{x,c1}$, is less sensitive to D for $D > -0.02$ compared to the natural convection boundary, and hence $Ri_{x,c2}$. Therefore, the width of the mixed convection regime is affected most by the location of the natural convection boundary. These results can also be realized by reference to Fig. 9(b). In general, for a given Gr_x, the Re_x range that identifies the mixed convection regime increases with decreasing suction and increasing injection. Likewise, the change from the forced convection regime to the natural convection regime, for a given

Table 2
Range of Richardson number (Ri_x) for the various convection regimes showing the effect of Pr and D for $B = 10^{-2}$

Pr	D	Forced convection	Mixed convection	Natural convection
0.1	−0.10	$Ri_x < 0.107$	$0.107 \leqslant Ri_x \leqslant 0.835$	$Ri_x > 0.835$
0.1	−0.05	$Ri_x < 0.107$	$0.107 \leqslant Ri_x \leqslant 1.43$	$Ri_x > 1.43$
0.1	−0.02	$Ri_x < 0.109$	$0.109 \leqslant Ri_x \leqslant 2.25$	$Ri_x > 2.25$
0.1	−0.01	$Ri_x < 0.110$	$0.110 \leqslant Ri_x \leqslant 2.66$	$Ri_x > 2.66$
0.1	0.00	$Ri_x < 0.110$	$0.110 \leqslant Ri_x \leqslant 3.27$	$Ri_x > 3.27$
0.1	0.01	$Ri_x < 0.111$	$0.111 \leqslant Ri_x \leqslant 4.13$	$Ri_x > 4.13$
0.1	0.02	$Ri_x < 0.112$	$0.112 \leqslant Ri_x \leqslant 5.43$	$Ri_x > 5.43$
0.1	0.05	$Ri_x < 0.117$	$0.117 \leqslant Ri_x \leqslant 17.7$	$Ri_x > 17.7$
1.0	−0.10	$Ri_x < 0.245$	$0.245 \leqslant Ri_x \leqslant 1.76$	$Ri_x > 1.76$
1.0	−0.05	$Ri_x < 0.142$	$0.142 \leqslant Ri_x \leqslant 4.93$	$Ri_x > 4.93$
1.0	−0.02	$Ri_x < 0.118$	$0.118 \leqslant Ri_x \leqslant 13.0$	$Ri_x > 13.0$
1.0	−0.01	$Ri_x < 0.112$	$0.112 \leqslant Ri_x \leqslant 20.4$	$Ri_x > 20.4$
1.0	0.00	$Ri_x < 0.107$	$0.107 \leqslant Ri_x \leqslant 37.2$	$Ri_x > 37.2$
1.0	0.01	$Ri_x < 0.103$	$0.103 \leqslant Ri_x \leqslant 79.5$	$Ri_x > 79.5$
1.0	0.02	$Ri_x < 0.100$	$0.100 \leqslant Ri_x \leqslant 217$	$Ri_x > 217$
1.0	0.03	$Ri_x < 0.096$	$0.096 \leqslant Ri_x \leqslant 1240$	$Ri_x > 1240$
10	−0.10	$Ri_x < *$	$* \leqslant Ri_x \leqslant 0.360$	$Ri_x > 0.360$
10	−0.05	$Ri_x < *$	$* \leqslant Ri_x \leqslant 1.41$	$Ri_x > 1.41$
10	−0.02	$Ri_x < *$	$* \leqslant Ri_x \leqslant 8.87$	$Ri_x > 8.87$
10	−0.01	$Ri_x < 4.86$	$4.86 \leqslant Ri_x \leqslant 30.6$	$Ri_x > 30.6$
10	0.00	$Ri_x < 1.70$	$1.70 \leqslant Ri_x \leqslant 378$	$Ri_x > 378$
10	0.001	$Ri_x < 1.63$	$1.63 \leqslant Ri_x \leqslant 578$	$Ri_x > 578$
10	0.002	$Ri_x < 1.57$	$1.57 \leqslant Ri_x \leqslant 857$	$Ri_x > 857$
10	0.003	$Ri_x < 1.52$	$1.52 \leqslant Ri_x \leqslant 1233$	$Ri_x > 1233$

$*Ri_{x,c1}$ could not be obtained since the 5% criterion overshot the mixed convection results throughout the whole region.

Re_x, occurs over a range of Gr_x that increases with decreasing suction and increasing injection.

The effect of varying Pr is shown in Fig. 14(a) and (b) for $Pr = 0.1$ and 10, respectively, and for $B = 10^{-2}$ and $D = -0.02$. These are complemented by Fig. 13(b) for $Pr = 1$. The convection map for $Pr = 0.1$ is characterized by a relatively narrow mixed convection regime which, generally, widens with increasing Pr. Under the conditions presented in Fig. 14(b), the 5% criterion overshoots the mixed convection results. Accordingly, $Ri_{x,c1}$ cannot be determined and the forced and mixed convection regimes cannot be separated. Therefore, one may regard that the forced convection regime to extend to the natural convection boundary, or that the mixed convection regime to extend to low Ri_x.

The effect of varying B is shown in Fig. 15(a) and (b) for $B = 10^{-4}$ and 1, respectively, and for $Pr = 1$ and $D = -0.02$. These are complemented by Fig. 13(b) for $B = 10^{-2}$. Under the conditions presented in Fig. 15(a), the forced and mixed convection regimes cannot be separated for the same reason given for the results in Fig. 14(b). By comparing the results in Figs. 13(b) and 15(b), it is noted that for a given Gr_x, the Re_x range that identifies the mixed convection regime decreases with increasing B. Also, the change from the forced convection regime to the natural convection regime, for a given Re_x, occurs over a range of Gr_x that increases with B. Note that the width or height of the mixed convection band, as it looks on the figure, is not indicative of the actual range of values because of the logarithmic scales.

The above results along with other results for different values of Pr, B and D were summarized earlier in Tables 1–3. The convection regimes maps are useful in the sense that when $Ri_x < Ri_{x,c1}$, natural convection effects can be ignored; when $Ri_x > Ri_{x,c2}$, forced convection effects can be ignored. When $Ri_{x,c1} < Ri_x < Ri_{x,c2}$, the problem must be analyzed as a mixed convection situation. To the author's best knowledge, convection regimes maps of the moving plate problem (backward boundary layer) with suction or injection have not been previously developed.

3.6. Comparison with Blasius-type problem

It is of practical interest to compare the results of the continuously moving plate in an otherwise stationary fluid with those of the moving fluid over a stationary plate. For the latter problem, the boundary conditions correspond to $u = 0$ at $y = 0$ and $u = u_\infty$ as $y \to \infty$, cf. Eqs. (6) and (9), in which case the situation is simply transformed from a Sakiadis-type mixed convection problem to a Blasius-type mixed convection problem. Fig. 16 shows the critical Richardson number variation

Table 3
Range of Richardson number (Ri_x) for the various convection regimes showing the effect of Pr and D for $B = 1$

Pr	D	Forced convection	Mixed convection	Natural convection
0.1	−0.10	$Ri_x < 2.06$	$2.06 \leqslant Ri_x \leqslant$ **	$Ri_x >$ **
0.1	−0.05	$Ri_x < 2.07$	$2.07 \leqslant Ri_x \leqslant$ **	$Ri_x >$ **
0.1	−0.02	$Ri_x < 2.08$	$2.08 \leqslant Ri_x \leqslant$ **	$Ri_x >$ **
0.1	−0.01	$Ri_x < 2.08$	$2.08 \leqslant Ri_x \leqslant$ **	$Ri_x >$ **
0.1	0.00	$Ri_x < 2.08$	$2.08 \leqslant Ri_x \leqslant$ **	$Ri_x >$ **
0.1	0.01	$Ri_x < 2.08$	$2.08 \leqslant Ri_x \leqslant$ **	$Ri_x >$ **
0.1	0.02	$Ri_x < 2.09$	$2.09 \leqslant Ri_x \leqslant$ **	$Ri_x >$ **
0.1	0.05	$Ri_x < 2.09$	$2.09 \leqslant Ri_x \leqslant$ **	$Ri_x >$ **
1.0	−0.10	$Ri_x < 0.886$	$0.886 \leqslant Ri_x \leqslant 22.5$	$Ri_x > 22.5$
1.0	−0.05	$Ri_x < 0.866$	$0.866 \leqslant Ri_x \leqslant 29.2$	$Ri_x > 29.2$
1.0	−0.02	$Ri_x < 0.859$	$0.859 \leqslant Ri_x \leqslant 34.5$	$Ri_x > 34.5$
1.0	−0.01	$Ri_x < 0.855$	$0.855 \leqslant Ri_x \leqslant 36.8$	$Ri_x > 36.8$
1.0	0.00	$Ri_x < 0.854$	$0.854 \leqslant Ri_x \leqslant 39.5$	$Ri_x > 39.5$
1.0	0.01	$Ri_x < 0.852$	$0.852 \leqslant Ri_x \leqslant 41.9$	$Ri_x > 41.9$
1.0	0.02	$Ri_x < 0.849$	$0.849 \leqslant Ri_x \leqslant 45.4$	$Ri_x > 45.4$
1.0	0.05	$Ri_x < 0.848$	$0.848 \leqslant Ri_x \leqslant 56.2$	$Ri_x > 56.2$
10	−0.10	$Ri_x < 5.45$	$5.45 \leqslant Ri_x \leqslant 31.9$	$Ri_x > 31.9$
10	−0.05	$Ri_x < 2.12$	$2.12 \leqslant Ri_x \leqslant 82.0$	$Ri_x > 82.0$
10	−0.02	$Ri_x < 1.53$	$1.53 \leqslant Ri_x \leqslant 182$	$Ri_x > 182$
10	−0.01	$Ri_x < 1.40$	$1.40 \leqslant Ri_x \leqslant 254$	$Ri_x > 254$
10	0.00	$Ri_x < 1.29$	$1.29 \leqslant Ri_x \leqslant 381$	$Ri_x > 381$
10	0.01	$Ri_x < 1.19$	$1.19 \leqslant Ri_x \leqslant 586$	$Ri_x > 586$
10	0.02	$Ri_x < 1.14$	$1.14 \leqslant Ri_x \leqslant 860$	$Ri_x > 860$
10	0.05	$Ri_x < 0.905$	$0.905 \leqslant Ri_x \leqslant 2780$	$Ri_x > 2780$

**$Ri_{x,c2}$ could not be obtained since the 5% criterion overshot the mixed convection results throughout the whole region.

with Prandtl number for the two respective problems calculated for $B = 10^{-6}$. The solid lines show the present results for the moving plate situation and the dashed lines show the present results for the stationary plate situation. The lines designated by c1 represent $Ri_{x,c1}$ (border between forced convection and mixed convection), and the lines designated by c2 represent $Ri_{x,c2}$ (border between mixed convection and natural convection). It is noted that u_∞ is the free-stream velocity and that B and Ri_x for the case of the stationary plate are based on u_∞.

The present results are also compared with those calculated by Chen et al. [32], shown as circles in Fig. 16, and Lloyd and Sparrow [33], shown as squares, for the stationary plate problem; and those by Ramachandran et al. [34], shown as triangles, for the moving plate problem. These results are available only for the special case of an impermeable plate ($D = 0$) and all use the boundary layer approximations. The method of local similarity was used in [33], whereas the finite difference method was used in combination with the method of local non-similarity in [32,34] and the two solutions were matched with some error at Ri_x of 10. Nevertheless, despite these errors and the approximations inherent in the numerical solutions, the comparisons show a generally good agreement with the present results.

As to the comparison between the two classes of problems with regard to the effect of Pr on the width of the mixed convection regime (regions between the two solid lines and the two dashed lines, i.e. distance between $Ri_{x,c2}$ and $Ri_{x,c1}$ for a given Pr), the results presented in Fig. 16 show an interesting behavior. Firstly, $Ri_{x,c1}$ and $Ri_{x,c2}$ are more sensitive to change in Pr for the moving plate problem compared to the stationary plate problem. Secondly, and as a consequence of the first point, the extent of the mixed convection regime increases significantly with increasing Pr for the moving plate problem. For the stationary plate problem, the width of the mixed convection regime is generally much narrower for Pr greater than about 0.3 (note the use of the logarithmic scales). Further comparisons between the two respective situations in terms of the heat transfer rate were given in [26].

4. Conclusions

The heat transfer and friction characteristics along a continuously moving vertical sheet of extruded material were studied close to and far downstream from the extrusion slot. Uniform or non-uniform suction/injection was allowed at the surface. The numerical model, based

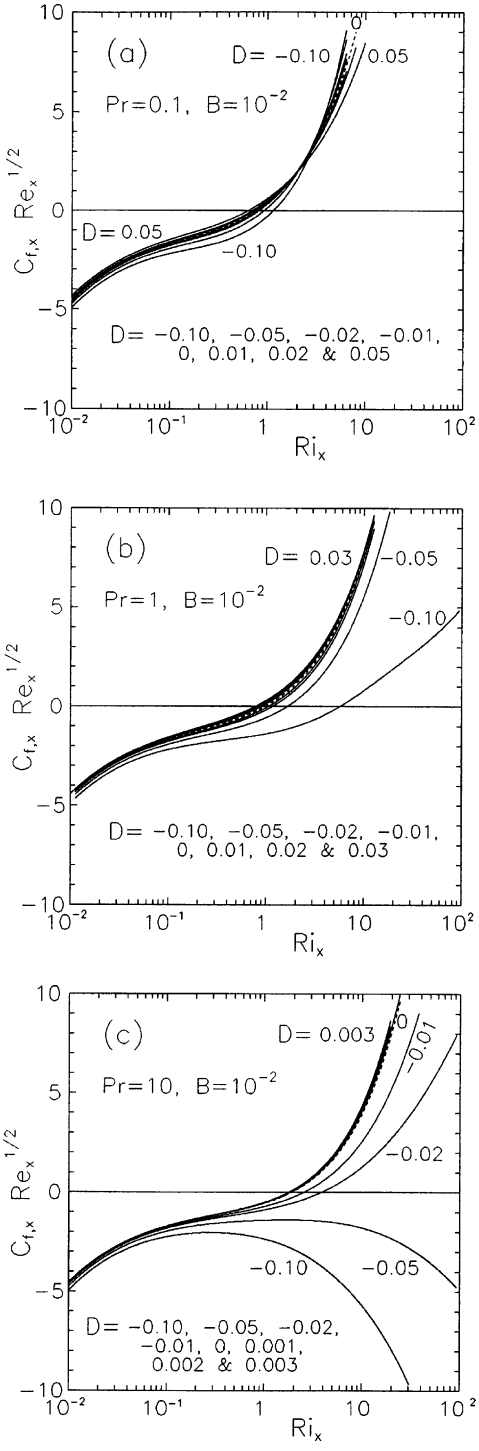

Fig. 11. Skin-friction coefficient variation with Richardson number for $B = 10^{-2}$ and different D: (a) $Pr = 0.1$, (b) $Pr = 1$, and (c) $Pr = 10$.

on a finite-volume procedure, was validated against published results available under special conditions and

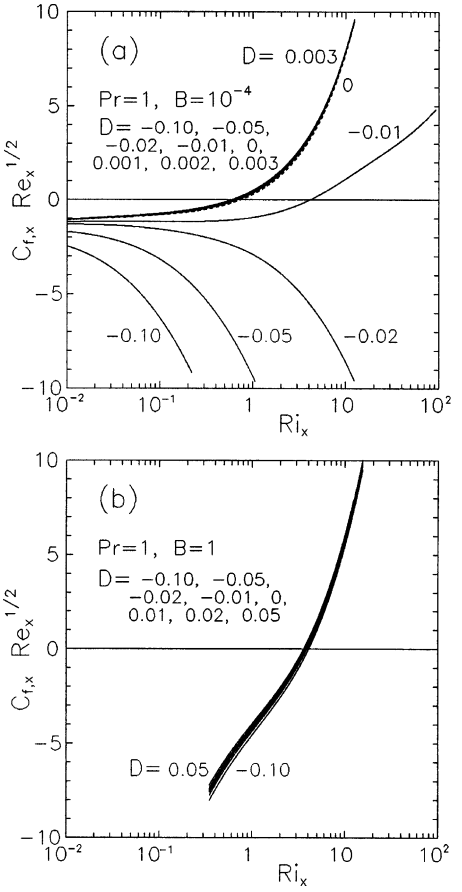

Fig. 12. Skin-friction coefficient variation with Richardson number for $Pr = 1$ and different D: (a) $B = 10^{-4}$, and (b) $B = 1$.

against exact solutions for asymptotic suction flows, and the comparisons showed an excellent agreement. Convection regimes have been delineated for different Pr, B and D. Under the conditions and range of parameters investigated, the following remarks are made.

(1) At low Ri_x, the heat transfer rates by the different convection modes are equal. This is attributed to the fact that diffusion dominates over both inertia and buoyancy in the region close to the extrusion slot. Little further downstream, the inertia forces start to show an effect as the stream-wise diffusion diminishes and, therefore, heat transfer enhancement over that of pure natural convection takes place. Further downstream, the buoyancy forces start to have an effect and the heat transfer rate by mixed convection increases above that by pure forced convection. At high Ri_x and for the case of uniform suction, the heat transfer rates by the different convection modes become, once again, equal due to reaching the asymptotic suction state.

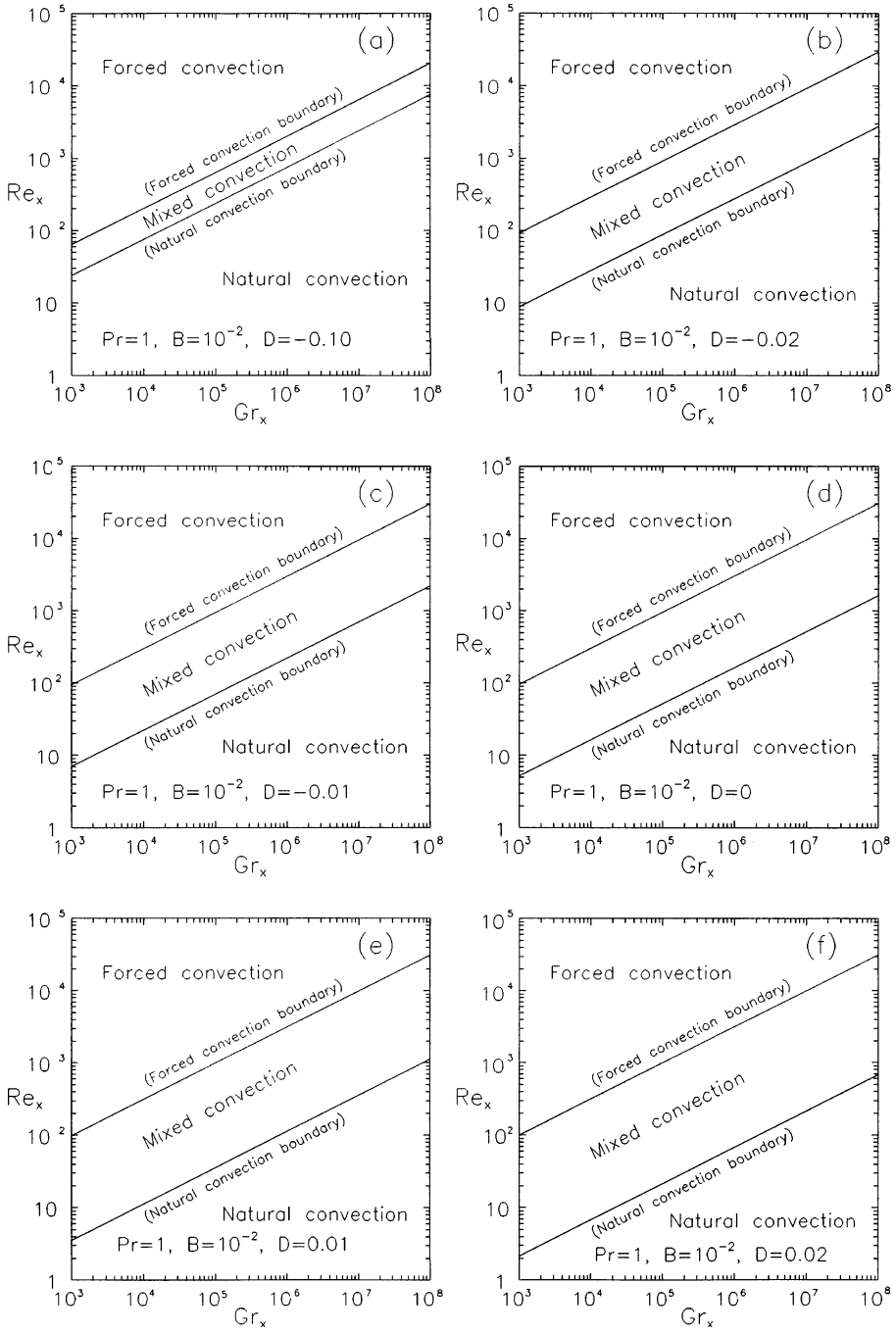

Fig. 13. Regimes of forced, mixed and natural convection for $Pr = 1$ and $B = 10^{-2}$: (a) $D = -0.10$, (b) $D = -0.02$, (c) $D = -0.01$, (d) $D = 0$, (e) $D = 0.01$, and (f) $D = 0.02$.

(2) The heat transfer rate drops sharply with distance in the forced-convection dominated region. The drop continues downstream but at a lower rate throughout the mixed and natural convection regions as the thermal boundary layer thickens. For the case of uniform suction, asymptotic temperature and velocity profiles are attained far downstream and the boundary layer thickness becomes constant. The ini-

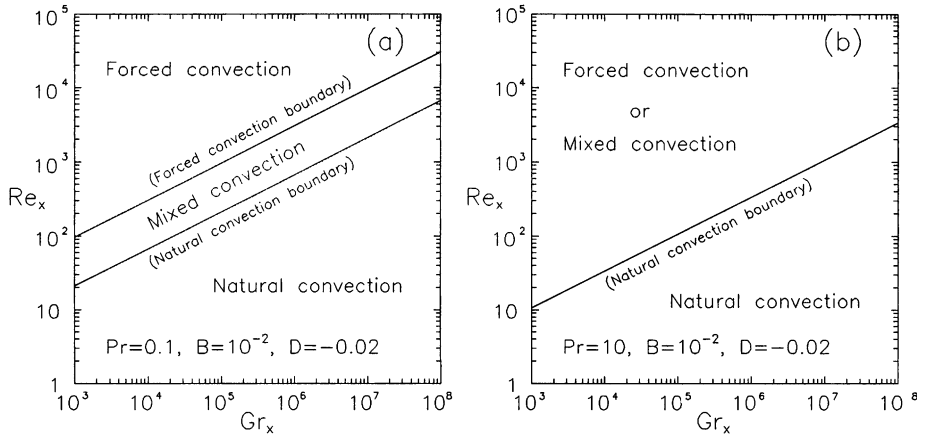

Fig. 14. Regimes of forced, mixed and natural convection for $B = 10^{-2}$ and $D = -0.02$: (a) $Pr = 0.1$, and (b) $Pr = 10$.

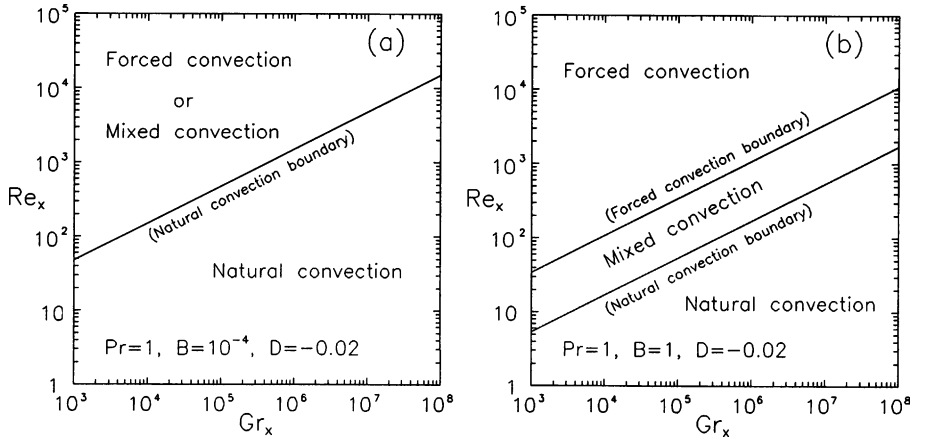

Fig. 15. Regimes of forced, mixed and natural convection for $Pr = 1$ and $D = -0.02$: (a) $B = 10^{-4}$, and (b) $B = 1$.

tial length required to reach the asymptotic suction state decreases with increasing suction.

(3) The heat transfer rate increases with increasing Pr, B and suction and decreases with increasing injection.
(4) At low Ri_x, the heat transfer results are less sensitive to Pr and D.
(5) The skin-friction coefficient changes sign when there is a velocity overshoot due to the effect of buoyancy. In the forced-convection dominated region, suction acts to increase the friction coefficient while injection acts to decrease it. However, the opposite behavior can take place in the mixed convection region depending upon the values of Pr, B and D.
(6) The location of the vanishing shear stress at the plate moves downstream with increasing Pr, B and suction.
(7) For the case of non-uniform suction or injection, critical values of Gr_x are determined for different D_N that distinguish the non-similar pure natural-convection region from the self-similar region. It is found that $Gr_{x,c}$ decreases with decreasing injection and increasing suction.
(8) In general, the extent of the mixed convection regime increases with increasing Pr, B and injection, and decreases with increasing suction.
(9) As a consequence of the last point and for a given Re_x, the transition from the forced convection regime to the natural convection regime occurs over a range of Gr_x that increases with increasing Pr, B and injection, and decreases with increasing suction.
(10) Comparison of results between the Sakiadis- and Blasius-type problems shows that the width of the mixed convection regime is more sensitive to change in Pr and widens significantly with increasing Pr for the Sakiadis-type problem.

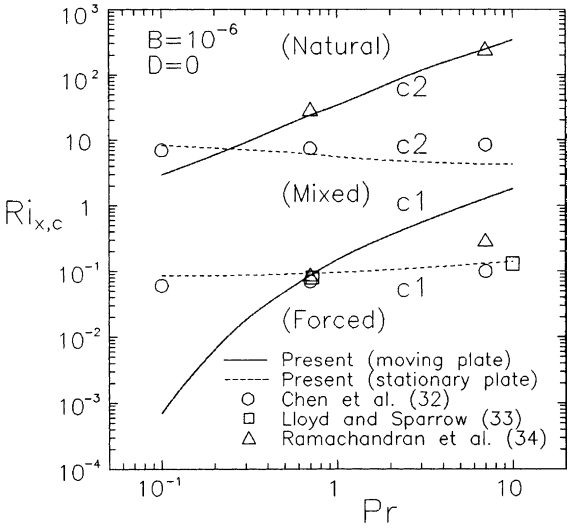

Fig. 16. Critical Richardson number variation with Prandtl number showing convection regimes and comparison between the Sakiadis- and Blasius-type problems for $B = 10^{-6}$ and $D = 0$.

References

[1] M.V. Karwe, Y. Jaluria, Fluid flow and mixed convection transport from a moving plate in rolling and extrusion processes, ASME J. Heat Transfer 110 (1988) 655–661.

[2] M.V. Karwe, Y. Jaluria, Numerical simulation of thermal transport associated with a continuously moving flat sheet in materials processing, ASME J. Heat Transfer 113 (1991) 612–619.

[3] B.C. Sakiadis, Boundary-layer behavior on continuous solid surfaces: I. Boundary-layer equations for two-dimensional and axisymmetric flow, AIChE J. 7 (1961) 26–28.

[4] B.C. Sakiadis, Boundary-layer behavior on continuous solid surfaces: II. The boundary layer on a continuous flat surface, AIChE J. 7 (1961) 221–225.

[5] F.K. Tsou, E.M. Sparrow, R.J. Goldstein, Flow and heat transfer in the boundary layer on a continuous moving surface, Int. J. Heat Mass Transfer 10 (1967) 219–235.

[6] V.M. Soundalgekar, T.V. Ramana Murty, Heat transfer in flow past a continuous moving plate with variable temperature, Warme Stoffubertrag. 14 (1980) 91–93.

[7] L.G. Grubka, K.M. Bobba, Heat transfer characteristics of a continuous stretching surface with variable temperature, ASME J. Heat Transfer 107 (1985) 248–250.

[8] D.R. Jeng, T.C.A. Chang, K.J. De Witt, Momentum and heat transfer on a continuous moving surface, ASME J. Heat Transfer 108 (1986) 532–539.

[9] M.E. Ali, Heat transfer characteristics of a continuous stretching surface, Warme Stoffubertrag. 29 (1994) 227–234.

[10] L.E. Erickson, L.T. Fan, V.G. Fox, Heat and mass transfer on a moving continuous flat plate with suction or injection, Ind. Eng. Chem. Fundam. 5 (1966) 19–25.

[11] V.G. Fox, L.E. Erickson, L.T. Fan, Methods for solving the boundary layer equations for moving continuous flat surfaces with suction and injection, AIChE J. 14 (1968) 726–736.

[12] P.S. Gupta, A.S. Gupta, Heat and mass transfer on a stretching sheet with suction or blowing, Can. J. Chem. Eng. 55 (6) (1977) 744–746.

[13] C.K. Chen, M. Char, Heat transfer over a continuous stretching surface with suction and blowing, J. Math. Anal. Appl. 135 (1988) 568–580.

[14] M.E. Ali, On thermal boundary layer on a power-law stretched surface with suction or injection, Int. J. Heat Fluid Flow 16 (4) (1995) 280–290.

[15] T.S. Chen, F.A. Strobel, Buoyancy effects on heat and mass transfer in boundary layer on a continuous, moving horizontal plate, Numer. Heat Transfer 3 (1980) 115–130.

[16] J.R. Fan, J.M. Shi, X.Z. Xu, Similarity solution of mixed convection over a horizontal moving plate, Heat Mass Transfer 32 (1997) 199–206.

[17] C.-H. Chen, Laminar mixed convection adjacent to vertical, continuously stretching sheets, Heat Mass Transfer 33 (1998) 471–476.

[18] M.E. Ali, F. Al-Yousef, Laminar mixed convection from a continuously moving vertical surface with suction or injection, Heat Mass Transfer 33 (4) (1998) 301–306.

[19] J. Fan, J. Shi, X. Xu, Similarity solution of free convective boundary-layer behavior at a stretching surface, Heat Mass Transfer 35 (1999) 191–196.

[20] A. Moutsoglou, T.S. Chen, Buoyancy effects in boundary layers on inclined, continuous, moving sheets, ASME J. Heat Transfer 102 (1980) 371–373.

[21] F.A. Strobel, T.S. Chen, Buoyancy effects on heat and mass transfer in boundary layers adjacent to inclined, continuous, moving sheets, Numer. Heat Transfer 3 (1980) 461–481.

[22] C.-H. Chen, Mixed convection cooling of a heated, continuously stretching surface, Heat Mass Transfer 36 (2000) 79–86.

[23] T.S. Chen, B.F. Armaly, Mixed convection in external flow, in: S. Kakac, R.K. Shah, W. Aung (Eds.), Handbook of Single-Phase Convective Heat Transfer, Wiley, New York, 1987, pp. 14.1–14.35 (Chapter14).

[24] B.H. Kang, Y. Jaluria, Heat transfer from continuously moving material in channel flow for thermal processing, J. Thermophys. Heat Transfer 8 (3) (1994) 546–554.

[25] S.A. Al-Sanea, M.E. Ali, The effect of extrusion slit on the flow and heat-transfer characteristics from a continuously moving material with suction or injection, Int. J. Heat Fluid Flow 21 (1) (2000) 84–91.

[26] S.A. Al-Sanea, Convection regimes and heat transfer characteristics along a continuously moving heated vertical plate, Int. J. Heat Fluid Flow, in press.

[27] W.M. Kays, M.E. Crawford, Convective Heat and Mass Transfer, third ed., McGraw-Hill, New York, 1993 (Chapter 17).

[28] S.V. Patankar, D.B. Spalding, A calculation procedure for heat, mass and momentum transfer in three-dimensional parabolic flows, Int. J. Heat Mass Transfer 15 (1972) 1787–1806.

[29] W.M. Pun, D.B. Spalding, A general computer program for two-dimensional elliptic flows, Report No. HTS/76/2, Department of Mechanical Engineering, Imperial College, London, 1977.

[30] S.A. Al-Sanea, W.M. Pun, D.B. Spalding, Computation of two-dimensional elliptic flows, including heat transfer, in: K. Morgan, C. Taylor, C.A. Brebbia (Eds.), Computer Methods in Fluids, Pentech Press, London, 1980, pp. 217–256.

[31] R. Eichhorn, The effect of mass transfer on free convection, ASME J. Heat Transfer 82 (1960) 260–263.

[32] T.S. Chen, B.F. Armaly, N. Ramachandran, Correlations for laminar mixed convection flows on vertical, inclined, and horizontal flat plates, ASME J. Heat Transfer 108 (1986) 835–840.

[33] J.R. Lloyd, E.M. Sparrow, Combined forced and free convection flow on vertical surfaces, Int. J. Heat Mass Transfer 13 (1970) 434–438.

[34] N. Ramachandran, T.S. Chen, B.F. Armaly, Mixed convection from vertical and inclined moving sheets in a parallel freestream, J. Thermophys. 1 (3) (1987) 274–281.